



Competitive anion/anion interactions on copper surfaces relevant for Damascene electroplating

N.T.M. Hai^a, T.T.M. Huynh^a, A. Fluegel^b, M. Arnold^b, D. Mayer^b, W. Reckien^c, T. Bredow^c, P. Broekmann^{a,b,*}

^a Department of Chemistry and Biochemistry, University of Bern, Freiestr. 3, Bern, Switzerland

^b BASF SE, Global Business Unit Electronic Materials, 67056 Ludwigshafen, Germany

^c Mulliken Center for Theoretical Chemistry, University of Bonn, Beringstr. 4, 53115 Bonn, Germany

ARTICLE INFO

Article history:

Received 13 March 2012

Accepted 15 March 2012

Available online 23 March 2012

Keywords:

Copper Damascene process

Electroplating

Additive

STM

ABSTRACT

The competitive interaction of chloride and SPS (bis-(sodium-sulfopropyl)-disulfide) at Cu(100)/electrolyte model interfaces was studied by means of cyclic voltammetry in combination with in situ STM and DFT. This specific anion/anion interaction is of paramount importance for the suppressor ensemble deactivation in the context of the industrial Cu Damascene process used for the state-of-the-art on-chip metallization. It is the interplay between chemisorbed chloride and SPS which regulates the dissociative SPS adsorption on copper as the key step in the course of the surface-confined MPS (mercaptopropane sulfonic acid) production. The latter species is considered as the actual anti-suppressor (depolarizer) in context of the Cu Damascene process.

Under competitive conditions the chloride adsorbs and orders much faster on Cu(100) than the SPS. The resulting $c(2 \times 2)$ -Cl adlayer acts as an effective barrier for the dissociative SPS adsorption, at least under *non-reactive conditions*. Defect sites within the chloride matrix are identified as crucial pre-requisites for the dissociative SPS adsorption. Defects are generated under *reactive conditions* during copper dissolution or copper deposition due to rapid anion adsorption/desorption dynamics. As consequence of the SPS dissociation a mixed, defect-rich $c(2 \times 2)$ -Cl-MPS co-adsorption phase forms on Cu(100) where every second chloride species of the pristine $c(2 \times 2)$ -Cl adlayer is displaced by MPS units. This co-adsorption phase reveals an apparent $p(2 \times 2)$ symmetry in the STM experiment since only the sulfonic head groups of the MPS units are imaged while the S and the Cl species chemisorbed on the copper surface remain invisible at the “buried” interface.

The relevance of this surface reaction for the Cu Damascene process is discussed in detail.

© 2012 Elsevier Ltd. All rights reserved.

1. Introduction

One of the key steps in today's mass fabrication of logic and memory devices is the void-free metallization of vias and trenches by means of additive-assisted copper electroplating [1]. For that an unconventional growth mode is mandatory that is in literature often referred to as super-fill [1]. This process requires a low copper deposition rate at the wafer surface and the upper side-walls of those features in combination with an “accelerated” copper deposition at the feature bottom. The most common concept in the context of the so-called Cu Damascene process relies on the use of a two component additive package. It is typically the

non-uniform surface coverage of a suppressor additive ensemble (polarizer) and its specific antagonist (depolarizer) which regulates the differential copper deposition velocity inside and outside of those features. Such non-uniformity in the additive surface coverage results from a combination of shape evolution effects upon feature fill (anti-suppressor dominated effect) [2–5] in combination with the sophisticated additive transportation/adsorption kinetics (suppressor-dominated effect) [6,7].

Poly-alkylated glycols (PAGs) are the most common suppressor precursors [1,8–10] which, however, require chloride [10–13] and most likely Cu(I) [12] as co-additives in order to show a suppressing effect on the copper deposition kinetics. SPS (bis-(3-sulfopropyl)disulfide) is commonly used as specific antagonist for the PAG/Cl/Cu(I) suppressor ensemble. When accumulated at the surface SPS is capable to avoid the formation of the PAG/Cl/Cu(I) suppressor ensemble.

One possible approach to gain more insights into the underlying molecular-level mechanism of this suppressor deactivation

* Corresponding author at: Department of Chemistry and Biochemistry, University of Bern, Switzerland. Tel.: +41 31 631 4317.

E-mail addresses: peter.broekmann@iac.unibe.ch, broekman@thch.uni-bonn.de (P. Broekmann).

process consists in the substantial simplification of those complex systems by using single crystalline model substrates exposed to additive containing but copper-free electrolytes. This approach allows the use of advanced scanning probe techniques in combination with state-of-the-art DFT methods both providing information on surface effects of physisorbing and chemisorbing additives.

Of central interest for our surface science approach is the identification of those structural motifs at the copper/electrolyte interface that contribute to the specific anti-suppressing action of the SPS.

One of the first scanning probe studies on the interaction of SPS and related derivatives with single crystalline copper surfaces was given by Taubert et al. [14]. This study reports an extremely slow SPS adsorption on Cu(1 1 1) due to the slow displacement of the ordered sulfate/water co-adsorption layer by the SPS. In this respect one can consider the pristine sulfate/water co-adsorption phase as an extra barrier for the SPS adsorption on copper. No lateral ordering within the formed MPS and SPS over-layers were resolved in this study [14].

However, industrial plating formulations typically contain strongly adsorbing chloride anions that are known to easily displace sulfate from the copper surface. Under more realistic conditions the SPS has therefore to compete with chloride for adsorption sites on copper. The competitive SPS/chloride adsorption was first addressed by Bae et al. using chloride-modified Cu(1 0 0) as model substrate [15]. No significant change in the surface structure of the pristine $c(2 \times 2)$ -Cl was observed in their in situ STM experiments when SPS was present in the electrolyte. From this observation it was concluded that the chloride lattice acts as an effective barrier for the SPS adsorption on Cu(1 0 0) similar to the sulfate/water co-adsorption layer described by Taubert et al. [14].

In one of the most recent contributions on the competitive SPS/Cl adsorption on Cu(1 0 0) Moffat et al. report a layer of physisorbed and laterally mobile SPS on-top of an intact $c(2 \times 2)$ -Cl lattice revealing a plurality of SPS adsorption configurations [16]. This layer of physisorbed SPS was not observed by Bae et al. [15] most likely due to the more drastic tunneling conditions (lower tunneling resistance) and low SPS concentrations used in this previous study that did not allow the imaging of weakly physisorbed SPS on the $c(2 \times 2)$ -Cl lattice.

Shifting the electrode potential close to or into the regime of the structural break-down of the $c(2 \times 2)$ -Cl lattice allows the SPS to adsorb on the bare copper surface involving the cleavage of the disulfide group. A $p(2 \times 2)$ -MPS (mercaptopropane sulfonic acid) layer was described by Moffat et al. as the final product of the SPS dissociation similar to the one reported for (bi)sulfide adsorption on Cu(1 0 0) [16,17]. Note, however, this potential regime is less relevant for the Damascene process that is commonly conducted at low current densities ranging from 4 to 10 mA/cm² [18] within a potential regime where a saturation monolayer of chloride is expected.

In this present study we will address the competitive SPS/Cl interaction demonstrating that SPS rapidly adsorbs and dissociates on copper even in the presence of a $c(2 \times 2)$ -Cl lattice, provided the copper/electrolyte interface is under *reactive conditions* involving rapid anion desorption and re-adsorption dynamics.

2. Experimental

Cyclic voltammetric experiments were performed in the electrochemical cell of the in situ STM (Scanning Tunneling Microscopy) set-up in order to facilitate the correlation between electrochemical and STM data. All potentials given in the text refer to a RHE (Reversible Hydrogen Electrode). STM experiments were carried

out using a Bonn-type STM which is described elsewhere in more detail [19].

Single crystalline Cu(1 0 0) (MaTeck GmbH, Germany) served in this study as model copper substrate. Prior to each experiment the copper surface need to be etched for the removal of the native oxide film according to the procedure described in Ref. [20].

STM and voltammetric experiments were conducted in 10 mM HCl serving as supporting electrolyte. All electrolyte solutions were deoxygenated with Ar gas before use.

SPS (bis-(sodium-sulfopropyl)-disulfide) and MPS (mercaptopropane sulfonic acid sodium salt) were purchased from Raschig and used without further purification. Note that both MPS and SPS are present in the electrolyte in their protonated and de-protonated form. Their pK_a values were determined to be $pK_a(\text{MPS}) = 1.68$ and $pK_a(\text{SPS}) = 1.34$.

The SPS adsorption on the chloride-terminated and bare Cu(1 0 0) surface was further studied by means of computational methods using periodic plane-wave density-functional theory (DFT) calculations with the VASP program package [21–23]. We employed the PBE exchange-correlation functional [24] in combination with the projector augmented wave method to account for the core electrons [25]. A cut-off energy of 400 eV for the plane-wave valence basis and a Monkhorst-Pack integration set-up with a $(3 \times 3 \times 1)$ k -point mesh was chosen. In all cases convergence tests showed that further increase of these accuracy parameters do not significantly alter the results. We applied a implementation [26] of Grimme's dispersion correction (DFT-D2) [27], since dispersion interaction – which is not correctly described by standard Kohn-Sham-DFT methods – plays a significant role in the molecule–surface interaction, as will be discussed in Section 3.3. Within this approach the energy $E_{\text{DFT-D2}}$ is the sum of the Kohn-Sham energy $E_{\text{KS-DFT}}$ and an empirical correction term E_{D2} according to:

$$E_{\text{DFT-D2}} = E_{\text{KS-DFT}} + E_{\text{D2}} \quad (1)$$

$$E_{\text{D2}} = -s_6 \sum_{i=1}^{N-1} \sum_{j=i+1}^N \frac{C_6^{ij}}{R_{ij}^6} f_{\text{dmp}}(R_{ij}) \quad (2)$$

C_6^{ij} is a dispersion coefficient for atom pair ij which is calculated from C_6 parameters for atoms i and j according to:

$$C_6^{ij} = \sqrt{C_6^i \cdot C_6^j} \quad (3)$$

R_{ij} represents the distance between the atoms of the ensemble. $s_6 = 0.75$ is a global scaling factor optimized for the PBE functional [27].

In order to avoid near-singularities for small distances the following damping function is introduced:

$$f_{\text{dmp}}(R_{ij}) = \frac{1}{1 + e^{-d(R_{ij}/R_r - 1)}} \quad (4)$$

R_r is the sum of modified atomic van-der-Waals radii, and d is a global parameter [27].

We studied both the SPS and MPS adsorption on the chloride-covered Cu(1 0 0) surface with a nominal chloride saturation coverage of $\Theta = 0.5$ ML and on defects within the $c(2 \times 2)$ -Cl matrix. These results are compared with the dissociative SPS adsorption on the blank, chloride-free Cu(1 0 0) surface.

The Cu surface was modeled with a $\begin{pmatrix} 4 & 4 \\ 3 & -3 \end{pmatrix}$ super-cell containing three layers of Cu. The $c(2 \times 2)$ -Cl adlayer was constructed according to Ref. [28] by placing twelve Cl atoms above the fourfold hollow positions of the surface super-cell. Defects in the chloride matrix were created by removing two Cl atoms from the super-cell.

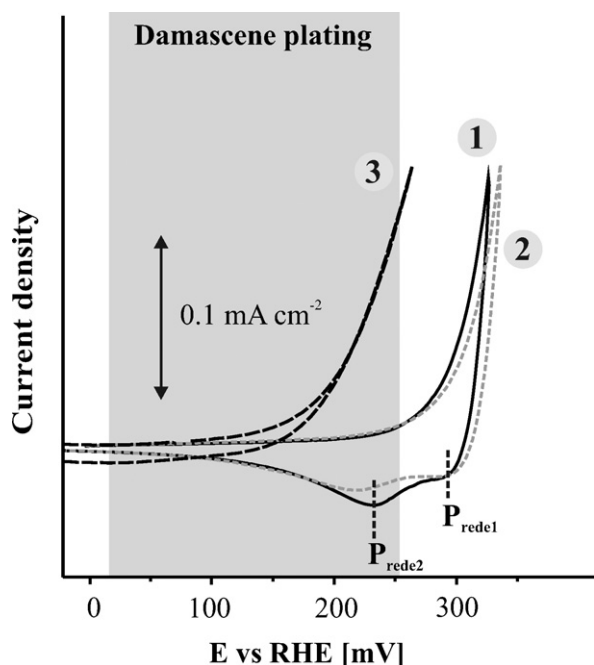


Fig. 1. Voltammograms demonstrating the influence of chloride, SPS and MPS on the voltammetric behavior of Cu(1 0 0). CV1: Cu(1 0 0) in 10 mM HCl; CV2: Cu(1 0 0) in 10 mM HCl + 1 mM SPS; CV3: Cu(1 0 0) in 10 mM HCl + 1 mM MPS $dE/dt = 10$ mV/s.

The first two atomic layers of the Cu(1 0 0) slab were relaxed in the adsorption calculations while the atoms of the third layer were kept at their bulk-like positions. The vacuum distance between the Cu surfaces was set to 2.15 Å. The SPS and MPS molecules were saturated with hydrogen atoms in our computational study in order to avoid charged cells.

For our calculations we did not include the liquid electrolyte into the model.

3. Results

3.1. Electrochemical characterization

Fig. 1 shows the cyclic voltammograms (CVs) of Cu(1 0 0) in the blank (10 m HCl) and the SPS or MPS containing electrolytes. We focus our considerations on the anodic part of those CVs including the double layer regime, the anodic Cu dissolution and the subsequent Cu re-deposition reaction since this potential regime is most relevant for the industrial Cu Damascene process. The potential range typically used for the Cu Damascene process is indicated in **Fig. 1**. CV1 displays the dissolution/re-deposition characteristics of Cu(1 0 0) in pure 10 mM HCl electrolyte and agrees well with literature [29,30]. A typical feature of this CV is a re-deposition peak in the reverse potential sweep that is split into two sub-peaks P_{rede1} and P_{rede2} . This characteristic is most likely related to the sequential reduction of Cu(II) to Cu(0) via Cu(I) intermediates when chloride anions are present. Note this splitting does not appear in the pure sulfuric acid electrolyte [30]. Interesting to note is that there is almost no impact of SPS on the dissolution/re-deposition characteristics when chloride is present (CV2 in **Fig. 1**). Slightly affected by the SPS is the Cu dissolution reaction that gets upward-shifted while the re-deposition peaks in the reverse scan are slightly damped. The overall shape of the CV remains, however, unchanged which is indicative for chloride anions that dominate the competitive anion adsorption, at least in the first cycles in the CV experiment. Chloride anions apparently adsorb much faster on Cu(1 0 0) than the SPS.

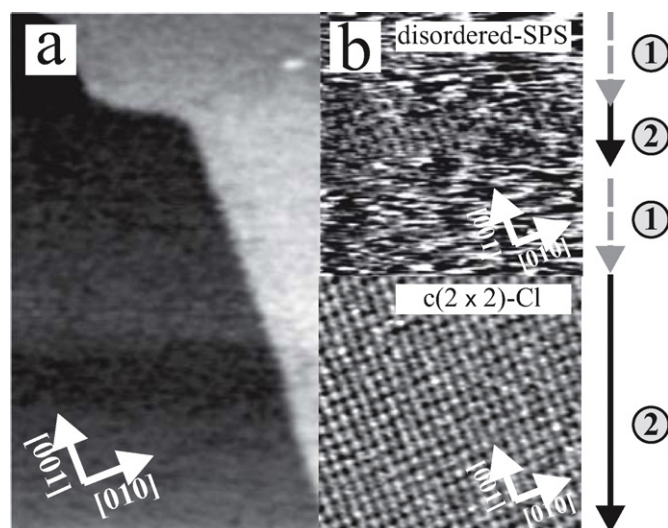


Fig. 2. STM data on the initial stage of SPS adsorption (physisorption) in the presence of a $c(2 \times 2)$ -Cl adlayer, (a) $58 \text{ nm} \times 28 \text{ nm}$, $E_{\text{work}} = +100$ mV vs. RHE, $I_t = 1$ nA, $U_b = 120$ mV; (b) $7.5 \text{ nm} \times 15 \text{ nm}$, $E_{\text{work}} = +100$ mV vs. RHE, $U_b = 80$ mV, the tunneling current was varied between $I_t = 0.1$ nA (interval 1) and $I_t = 5$ nA (interval 2).

Dosing MPS to the 10 mM HCl solution leads to significant changes in the voltammetric characteristics. Affected by the MPS is the oxidative copper dissolution that is shifted to lower potentials by about 150 mV clearly pointing to the corrosive effect of MPS. Most intriguing is, however, the absence of any pronounced re-deposition peak in the reverse potential sweep. Both effects can be rationalized in terms of Cu(I) intermediates that are stabilized by complexing MPS ligands most likely via their thiol functionality (see Section 4).

3.2. Structural characterization by means of STM

From literature it is well known that chloride forms a laterally ordered $c(2 \times 2)$ -Cl adlayer phase on Cu(1 0 0) [29–32]. Even under competitive adsorption conditions it is indeed the chloride that adsorbs and orders much faster on Cu(1 0 0) than the SPS thus resulting into a fully intact $c(2 \times 2)$ -Cl phase. **Fig. 2** shows the initial surface condition after such a competitive Cl/SPS adsorption at $E_{\text{work}} = +100$ mV. Morphological features such as the preferential step orientation along the substrate (1 0 0) directions are well developed and indicative for the presence of the $c(2 \times 2)$ -Cl phase [30,33]. The “fuzzy” appearance of the STM images under soft tunneling conditions (**Fig. 2a**) could be rationalized in terms of structurally intact SPS molecules that are physisorbed and laterally mobile on-top of the underlying $c(2 \times 2)$ -Cl lattice. This finding is consistent with both the STM work by Bae et al. [15] and by Moffat et al. [16]. Under more drastic tunneling conditions the tunneling tip easily removes such physisorbed SPS species upon scanning giving rise to the appearance of the $c(2 \times 2)$ -Cl lattice (**Fig. 2b**). Removal and re-appearance of the SPS physisorption layer in the STM experiment is completely reversible. It should be noted that $c(2 \times 2)$ -Cl phase exposed to an electrolyte that contains a mixture of Cl and SPS remains stable even in the potential range between $E_{\text{work}} = 0$ mV and $E_{\text{work}} = +200$ mV. This finding confirms the structurally intact chloride adlayer as an effective barrier for the adsorptive SPS dissociation [15,17].

Generally there are two experimental approaches toward the acceleration of the adsorptive SPS dissociation in the presence of chemisorbed chloride.

The first approach is based on an increase of the point defects within the chloride matrix by lowering the potential-dependent

chloride surface coverage as reported by Moffat et al. [16,17]. STM data clearly indicate the presence of individual SPS/MPS species within the chloride matrix as the initial stage of the co-adsorption phase formation [34]. Interestingly these MPS and SPS species reveal an extremely low lateral mobility within the chloride matrix quite in contrast to (bi)sulfide anions co-adsorbed in the same $c(2 \times 2)$ -Cl matrix [35]. Video-rate STM is typically required to follow the lateral motion of individual (bi)sulfide co-adsorbates within the chloride matrix [35].

Passing a certain threshold in the chloride surface coverage gives rise to the structural breakdown of the $c(2 \times 2)$ -Cl lattice. The resulting 2D lattice gas of laterally mobile chloride anions [36] does not represent an effective barrier so that SPS gets nearly full excess to the metallic copper surface and readily dissociates into MPS monomers [16].

An alternative and for the Damascene process more relevant approach to generate defects within the chloride matrix makes use of either copper dissolution or copper deposition. Under these *reactive conditions* defects appear within the pre-existing chloride matrix at nucleation centers and growth fronts of the emerging copper deposit. For the nucleation and growth of copper the chemisorbed chloride has to desorb temporarily from the copper surface. These anion desorption/re-adsorption dynamics allow the physisorbed SPS to adsorb on the metallic copper surface and to dissociate into monomeric MPS even at high potentials. Based on this concept we produced MPS/Cl co-adsorption phases by repeating cycles of copper dissolution/re-deposition in the presence of the mixed Cl/SPS electrolyte. For this procedure we did not exceed anodic current densities of $J = 0.2 \text{ mA/cm}^2$. 10 cycles were sufficient to obtain MPS/Cl co-adsorption phases as presented in Fig. 3a–c. Note that current densities used for the fill of Damascene features are typically in the range of $J = 4\text{--}10 \text{ mA/cm}^2$.

Patches of ordered adlayer domains reveal a local $p(2 \times 2)$ symmetry with an apparent nearest neighbor distances of $\text{NND} = 5.1 \text{ \AA} \pm 0.1 \text{ \AA}$. We assign the STM dots in Fig. 3b and c to the terminating sulfonic acid/sulfonate head groups of chemisorbed MPS entities. The nominal surface coverage of $\Theta_{\text{MPS}} = 0.25 \text{ ML}$ would correspond to a fully developed $p(2 \times 2)$ -MPS over-layer. However, patches of the *apparent* $p(2 \times 2)$ -MPS phase are separated by darker lines that can be rationalized in terms of “light” domain walls (Fig. 3a–c). Below we will provide further experimental evidence for the presence co-adsorbed chloride at the “buried” copper interface. Within this picture we interpret the dark lines in the STM images as chloride-rich, light domain walls. Their presence indicates an *actual* MPS surface coverage that is slightly smaller than the *nominal* surface coverage of $\Theta_{\text{MPS}} = 0.25 \text{ ML}$. Fig. 3d shows a schematic structure model of the adlayer with the apparent $p(2 \times 2)$ symmetry of the sulfonic head groups that are imaged in the STM. The true symmetry of the adlayer is, however, a $c(2 \times 2)$ as indicated in Fig. 3e. Every second chloride anion of the pristine $c(2 \times 2)$ -Cl phase is supposed to be displaced by an MPS unit at the “buried” interface. The thiolate functionality thereby anchors the MPS to the underlying copper substrate.

Clear evidence for the adsorptive SPS dissociation comes from additional experiments where MPS was directly adsorbed on a chloride-modified Cu(100) surface (Fig. 3f–h). MPS is capable to displace chloride spontaneously leading to the same lateral surface structure as previously observed for the dissociative SPS adsorption (Fig. 3a–c).

Several morphological aspects support the hypothesis of a Cl/SPS co-adsorption lattice present at the buried copper interface. The preferred step-alignment along the substrate (100) directions typically corresponds to the closed packed rows of adsorbed species in a $c(2 \times 2)$ phase [29,30,33]. Fig. 4a displays the *apparent* $p(2 \times 2)$ adlayer symmetry with close packed sulfonate/sulfonic acid groups parallel to the substrate (110) directions. Substrate step edges are,

however, rotated by 45° with respect to these directions. Step edges parallel to those (100) directions are expected for the presence of a true $c(2 \times 2)$ phase [29,30,33]. Therefore we interpret the *apparent* $p(2 \times 2)$ phase as an MPS sub-lattice of the true $c(2 \times 2)$ -Cl-MPS co-adsorption phase (Fig. 3e).

For comparison we present in Fig. 4b STM images of a *true* $p(2 \times 2)$ adlayer [37] of the low coverage (bi)sulfide phase on Cu(100) with step edges indeed oriented parallel to the substrate (110) directions. In this particular case the morphological features correspond to the atomic-scale structure. This adlayer was obtained after exposure of Cu(100) to a (bi)sulfide containing electrolyte at potentials in the hydrogen evolution regime according to the preparation protocol reported by Spaenig et al. [37].

The same trend of step-stabilization along the (100) directions as in Fig. 4a can be observed at the on-set of the copper dissolution reaction when the $c(2 \times 2)$ -Cl-MPS co-adsorption phase is present (Fig. 5). Copper dissolution preferentially starts from the chloride-rich light domain walls within the MPS/Cl co-adsorption phase and proceeds along the (100) directions. The overall dissolution characteristics can be best described by a “pit-etching” mechanism. At higher dissolution rates the surface gets significantly roughened due to a copper removal rate at step edges that is comparably slow relative to the nucleation of new defects within substrate terraces. This effect is clearly due to the presence of the MPS that effectively blocks step edges thus converting the step-flow mechanism that is commonly observed in pure Cl-containing electrolytes [30] into a pit-etching mechanism (Fig. 5).

The breakdown of the $c(2 \times 2)$ -Cl phase takes typically place at potentials below $E_{\text{work}} = -200 \text{ mV}$. *Selective* chloride desorption from the $c(2 \times 2)$ -Cl-MPS phase starts at about $E_{\text{work}} = -170 \text{ mV}$ and leaves a disordered MPS layer behind (Fig. 6a). The order-disorder transition is (quasi)reversible. Sweeping the potential back to $E_{\text{work}} = 0 \text{ mV}$ leads to the chloride re-adsorption (Fig. 6b). With a certain time delay the $c(2 \times 2)$ -Cl-MPS co-adsorption phase (apparent $p(2 \times 2)$ -MPS phase) reappears.

3.3. Computational modeling of the dissociative SPS adsorption

The initial SPS adsorption on the intact $c(2 \times 2)$ -Cl lattice is basically a physisorption process (Fig. 7a and Table 1). The S–S bond remains fully intact with a bond length of $R(\text{S–S}) = 2.037 \text{ \AA}$ that is identical to the one of SPS in the non-adsorbed state. The calculated adsorption energy of about $E_{\text{ads}} = -43 \text{ kJ/mol}$ is entirely due to the empirical D2 correction (Table 1). It should be noted, however, that there are various other physisorption configurations possible with minimal differences in their adsorption energy. One can therefore assume a nearly barrier-free movement of the structurally intact physisorbed SPS on the chloride lattice (Fig. 2).

SPS dissociation on the intact $c(2 \times 2)$ -Cl lattice is endothermic by $+64 \text{ kJ/mol}$. In this respect our calculations clearly confirm the experimental observations of the $c(2 \times 2)$ -Cl monolayer acting as an effective barrier preventing SPS dissociation.

Table 1

Calculated adsorption energies E_{ads} in kJ/mol for systems presented in Fig. 7. Numbers of E_{ads} are calculated with respect to non-dissociated SPS (calculated dissociation energy: $E_{\text{ads}} = 250 \text{ kJ/mol}$) and the particular surface model. In the last column we give the approximated contribution of the empirical dispersion correction to the overall E_{ads} in %.

System	E_{ads} (kJ/mol)	D_2
SPS on $c(2 \times 2)$ -Cl (Fig. 7a)	–43	100
SPS within $c(2 \times 2)$ -Cl (Fig. 7b)	–70	100
MPS within $c(2 \times 2)$ -Cl (Fig. 7c)	–310	40
SPS on Cu(100) (Fig. 7d)	–157	50
MPS on Cu(100) (Fig. 7e)	–360	25

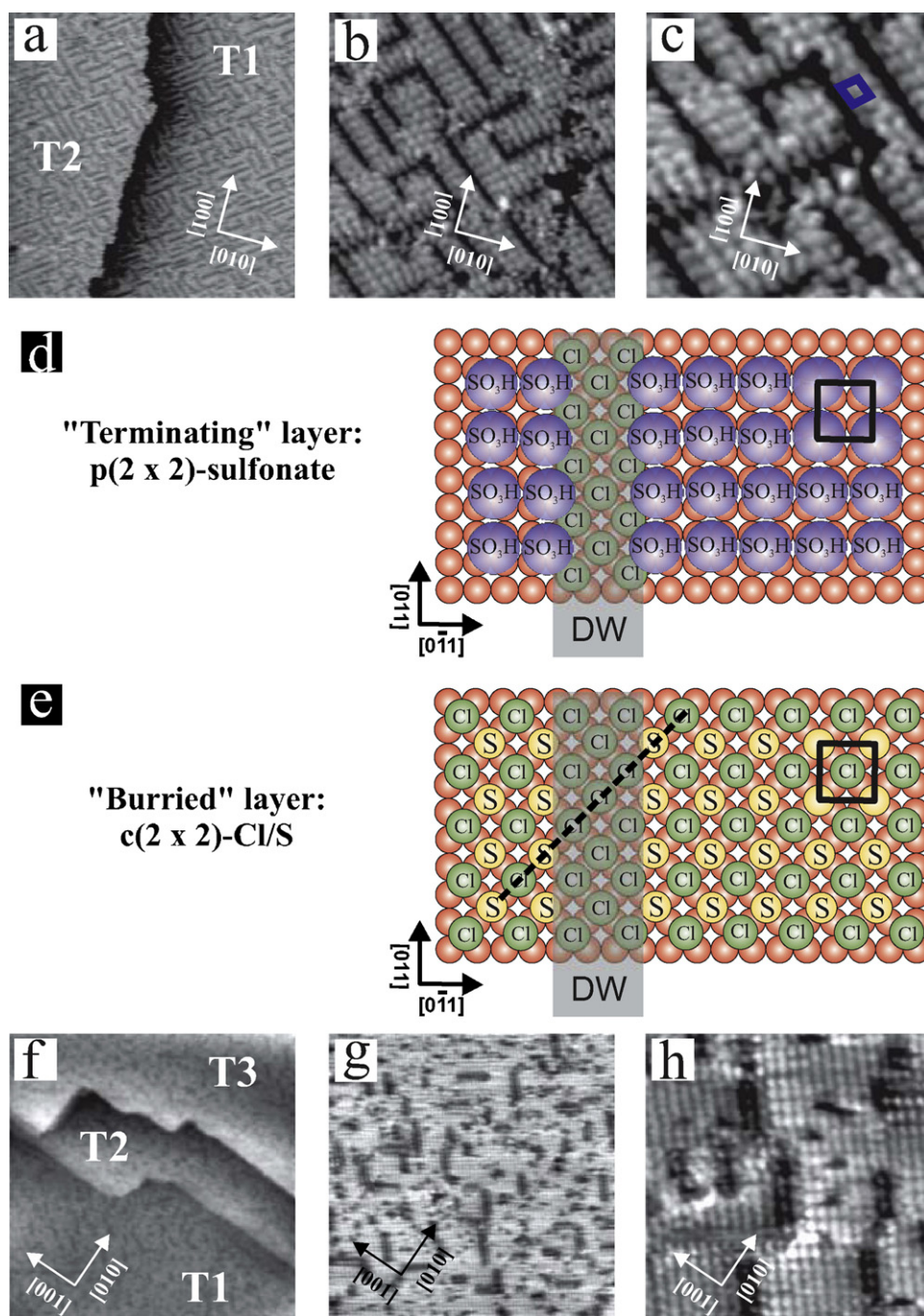


Fig. 3. (a)–(c) Defect-rich MPS/Cl co-adsorption layer on Cu(100) after 10 dissolution/re-deposition cycles in the presence of SPS in solution; (a) 56.1 nm \times 56.1 nm, $E_{\text{work}} = 0$ mV, $I_t = 0.3$ nA, $U_b = -143$ mV; (b) 12.5 nm \times 12.5 nm, $E_{\text{work}} = 0$ mV, $I_t = -143$ nA, $U_b = 0.3$ mV; (c) 8 nm \times 8 nm, $E_{\text{work}} = 0$ mV, $I_t = 0.3$ nA, $U_b = -143$ mV; (d) structure model of the *apparent* $p(2 \times 2)$ -MPS layer on Cu(100) as imaged in the STM experiment; (e) structure model of the *true* $c(2 \times 2)$ -Cl-S layer at the "buried" interface on Cu(100). (f)–(h) Defect-rich MPS/Cl co-adsorption layer on Cu(100) after competitive MPS/Cl adsorption on Cu(100), (f) 98.3 nm \times 93.3 nm, $E_{\text{work}} = +136$ mV, $I_t = 0.1$ nA, $U_b = 293$ mV; (g) 46.1 nm \times nm, $E_{\text{work}} = +136$ mV, $I_t = 0.1$ nA, $U_b = 293$ mV; (h) 11 nm \times 11 nm, $E_{\text{work}} = +136$ mV, $I_t = 0.1$ nA, $U_b = 293$ mV.

SPS dissociation, however, is facilitated at defect sites within the $c(2 \times 2)$ -Cl matrix starting with the initial physisorption of the non-dissociated SPS precursor leaving the S–S bond almost fully intact with $R(\text{S}–\text{S}) = 2.067$ Å (Fig. 7b). Two neighbored point defects within the $c(2 \times 2)$ -Cl matrix are required for such an initial SPS physisorption on copper. The interaction energy of SPS amounts to $E_{\text{ads}} = -70$ kJ/mol. Again, this initial SPS adsorption configuration is meta-stable. The physisorption is followed by the highly exothermic SPS dissociation within the $c(2 \times 2)$ -Cl matrix leaving two chemisorbed MPS entities behind both occupying fourfold

hollows of the Cu(100) lattice (Fig. 7c). The SPS adsorption energy on the defect in the $c(2 \times 2)$ -Cl matrix amounts to $E_{\text{ads}} = -310$ kJ/mol with respect to non-adsorbed SPS. This number corresponds to an MPS adsorption energy of $E_{\text{ads}} = -280$ kJ/mol if one considers $E_{\text{ads}} = 250$ kJ/mol for the breaking of the S–S bond. Driving force for the S–S bond rupture is therefore clearly the S–Cu bond formation. The Cu–S distance amounts to $d(\text{Cu}–\text{S}) = 1.366$ Å (Fig. 7c).

For comparison we present DFT results on the SPS adsorption on Cu(100) in the absence of chloride. The most stable configuration of adsorbed SPS is presented in Fig. 7d. Intact SPS adsorbs on

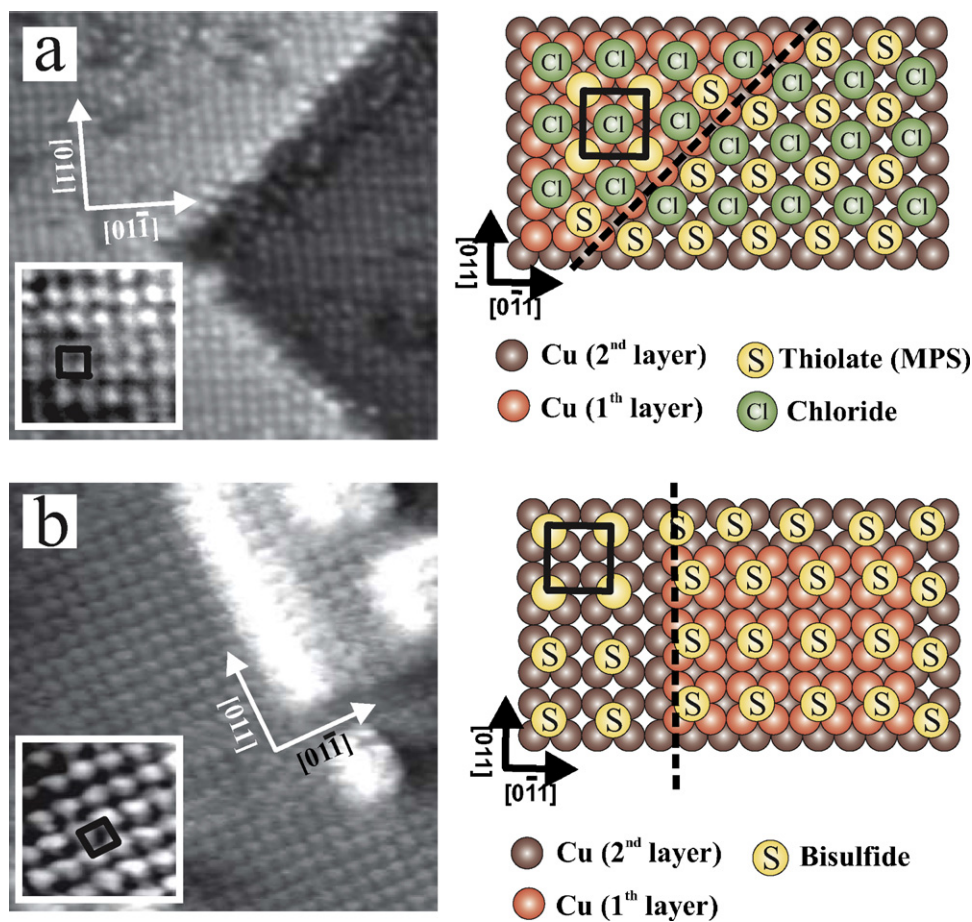


Fig. 4. Preferential step-alignment in the presence of the $c(2 \times 2)$ -Cl-MPS adlayer on Cu(100) (apparent $p(2 \times 2)$ -MPS layer) and the true $p(2 \times 2)$ -SH layer on Cu(100), (a) $14 \text{ nm} \times 14 \text{ nm}$, $E_{\text{work}} = +140 \text{ mV}$, $I_t = 0.1 \text{ nA}$, $U_b = 203 \text{ mV}$, the in-set shows a $3.4 \text{ nm} \times 3.4 \text{ nm}$ section of the apparent $p(2 \times 2)$ -MPS layer; (b) $12.6 \text{ nm} \times 12.6 \text{ nm}$, $E_{\text{work}} = -250 \text{ mV}$, $I_t = 3.5 \text{ nA}$, $U_b = 54 \text{ mV}$, the in-set shows a $2.3 \text{ nm} \times 2.3 \text{ nm}$ section of the true $p(2 \times 2)$ -SH layer.

the bare Cu(100) surface with both sulfur atoms in on-top positions. For the most stable conformer we find the center of the S–S bond in a bridging position with a calculated adsorption energy of $E_{\text{ads}} = -156 \text{ kJ/mol}$ (Fig. 7d and Table 1). However, an energetically almost equivalent structure motif with an S–S bond residing on a symmetric fourfold hollow site (model not shown) reveals only $\Delta E_{\text{ads}} = +5 \text{ kJ/mol}$ higher binding energy. In both cases dispersion interactions computed by the D2 correction contribute to the overall interaction energy of about 50%. However, the remaining 50% show that the SPS binding to the Cu(100) surface has significant covalent nature (Table 1).

The mixed covalent and dispersive nature of this S–S bonding to the metallic copper surface is further confirmed by an S–S bond of

the SPS that is slightly expanded (weakened) in the adsorbed state (Fig. 7d). The S–S bond length increases from $R(\text{S–S}) = 2.037 \text{ \AA}$ in the non-adsorbed SPS to $R(\text{S–S}) = 2.079 \text{ \AA}$ in the adsorbed state. The distance of the S–S disulfide group to the copper surface is slightly asymmetric with $d_1(\text{Cu–S}) = 2.459 \text{ \AA}$ and $d_2(\text{Cu–S}) = 2.420 \text{ \AA}$.

The adsorption configuration in Fig. 7d has to be considered as a meta-stable precursor for the chemisorptive SPS dissociation into two monomeric MPS entities on Cu(100) (see Fig. 7e). Any further lateral movement of the SPS on the copper surface instantaneous leads to the rupture of the S–S bond pointing to an almost barrier-free SPS dissociation on the bare Cu(100) surface. This reaction is highly exothermic by about $\Delta E_{\text{ads}} = -200 \text{ kJ/mol}$. Accordingly, the calculated adsorption energy amounts to $E_{\text{ads}} = -360 \text{ kJ/mol}$

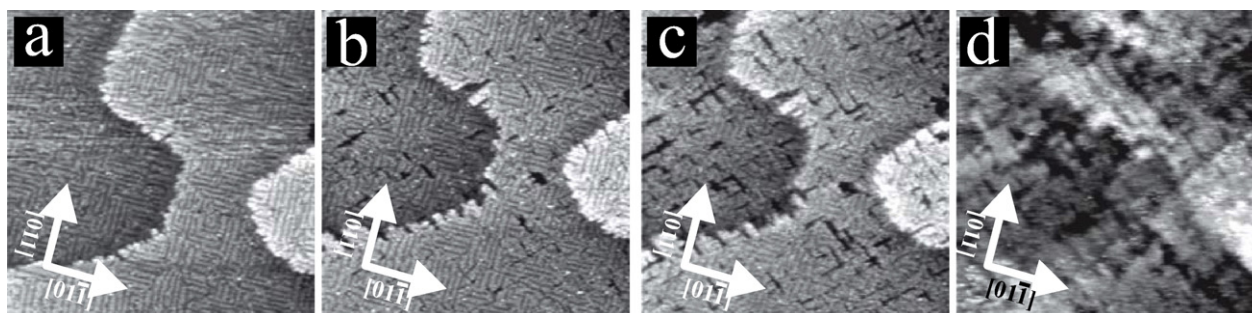


Fig. 5. Series of STM images showing the pit-etching dissolution mechanism in the presence of the $c(2 \times 2)$ -Cl-MPS adlayer. (a)–(d) $83 \text{ nm} \times 83 \text{ nm}$, $I_t = 0.4 \text{ nA}$, $U_b = -128 \text{ mV}$; (a) $E_{\text{work}} = +162 \text{ mV}$; (b) $E_{\text{work}} = +202 \text{ mV}$; (c) $E_{\text{work}} = +211 \text{ mV}$; (d) $E_{\text{work}} = +212 \text{ mV}$.

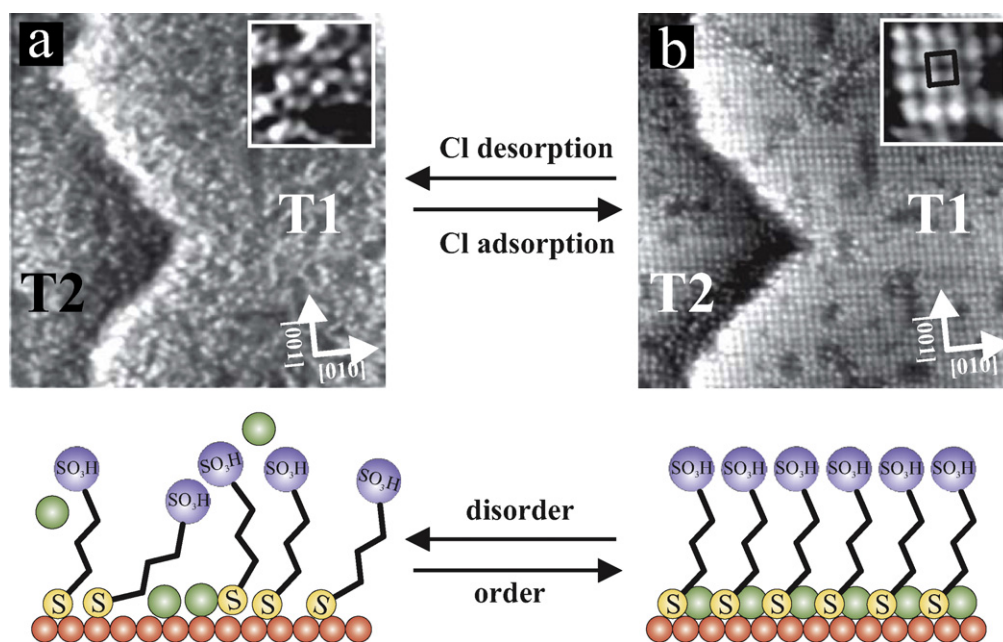


Fig. 6. Break-down of the lateral order in the $c(2 \times 2)$ -Cl-MPS adlayer due to *selective* chloride desorption, (a) $26.2 \text{ nm} \times 26.2 \text{ nm}$, $E_{\text{work}} = -193 \text{ mV}$, $I_t = 0.1 \text{ nA}$, $U_b = 203 \text{ mV}$ (the in-set shows a $2.4 \text{ nm} \times 2.4 \text{ nm}$ section of the *disordered* MPS layer); (b) $27.1 \text{ nm} \times 27.1 \text{ nm}$, $E_{\text{work}} = +140 \text{ mV}$, $I_t = 0.1 \text{ nA}$, $U_b = 171 \text{ mV}$ (the in-set shows a $2.4 \text{ nm} \times 2.4 \text{ nm}$ section of the *apparent* $p(2 \times 2)$ -MPS layer).

with respect to SPS in the non-adsorbed state. Preferred adsorption sites are fourfold hollows of the Cu(100) lattice. The distance of the sulfur to the copper surface for the adsorbed MPS amounts to $d(\text{Cu}-\text{S}) = 1.440 \text{ \AA}$ with a dominating 75% covalent nature of the bonding (Table 1). This covalent nature of the Cu–S bonding further results into an outward relaxation of those 4 copper atoms by about $\Delta z = 0.19 \text{ \AA}$.

4. Discussion

Although the Damascene process has to be considered as a key processing step in the state-of-the-art chip manufacturing our molecular level understanding of the underlying mechanisms of synergistic and antagonistic additive effects is still poor. Neither the exact molecular structure of the active PAG/Cu(I)/Cl suppressor ensemble is unambiguously solved nor the mechanism how the SPS antagonist deactivates this suppressor ensemble.

Very recently Moffat et al. proposed the 2D lattice-gas of structurally intact SPS on-top of the chloride adlayer (Figs. 2 and 7a) as physical origin for the observed “accelerating” or anti-suppressing effect of the SPS [16,17]. The SPS was assumed to disturb the interaction of the PAG to the chemisorbed chloride on the copper that is needed as essential co-additive in the resulting suppressor ensemble. In this picture the chemisorbed chloride takes over the role as specific linker between the PAG polymer and the copper surface [11,38]. SPS physisorbed on the chloride lattice is supposed to sterically hinder the access of the PAG to the chloride linker at the surface thus resulting into a disruption of the PAG surface complex. Our DFT studies indeed prove the SPS as weakly physisorbing on the Cl-terminated copper surface (Fig. 7a).

What makes this model particularly attractive is the assumption of an anti-suppressing species that remains laterally mobile. As demonstrated by our DFT calculations the calculated adsorption energy of structurally intact SPS of about $E_{\text{ads}} = -43 \text{ kJ/mol}$ is entirely due to the empirical D2 correction (Table 1) in combination with a nearly barrier-free movement of the structurally intact, physisorbed SPS on the chloride lattice. As pointed out by Josell et al. [39] such laterally mobile anti-suppressor species are

advantageous for the working of the Curvature Enhanced Accelerator Coverage (CEAC) model where the anti-suppressor species (accelerator, depolarizer) are supposed to float on top of the emerging copper surface as a crucial prerequisite for their accumulation inside the concave Damascene features upon fill.

However, there are essentially two drawbacks of this physisorption model left.

First, it does not explain why the SPS acts as specific antagonist with respect to the PAG suppressor chemistry. There are indeed only a few alternative anti-suppressor chemistries described in literature that are by far less effective than the SPS. If the deactivation of the PAG suppressor ensemble would indeed rely on a non-specific physisorption process one would expect more chemistries available showing a similar anti-suppressing behavior as the SPS.

Second, the physisorption model contradicts the experimentally observed sequence in the additive action under competitive adsorption conditions. This can be demonstrated by potentiometric Cu plating experiments where mixtures of chloride, PAG and SPS additives are dosed to a copper plating bath in an RDE configuration [40]. The intrinsic accelerating action of the chloride is by far the fastest process followed by the suppressing action of the PAG suppressor ensemble [40]. It is the deactivation of the PAG suppressor ensemble by the SPS that shown to be the slowest process [6,40]. This observation is a clear experimental hint for an anti-suppressor action of the SPS that requires an extra activation. This scenario is incompatible with an almost barrier-less SPS physisorption and subsequent lateral movement on the chloride-covered copper which has to be considered as fast.

We therefore propose a model that involves the physisorption as a first step in a more complex SPS surface reaction cycle that produces monomeric MPS as the actual anti-suppressor species in the course of this surface reaction. Fig. 8 summarizes our model. It can be considered as being in full agreement with both the CEAC model [2–4,41,42] and the time dependent transportation and adsorption model [6,7].

Chloride is actually the additive that adsorbs first on the copper surface as evidenced by our STM (Fig. 2) and chronopotentiometric experiments [40]. The particular role of chemisorbed chloride

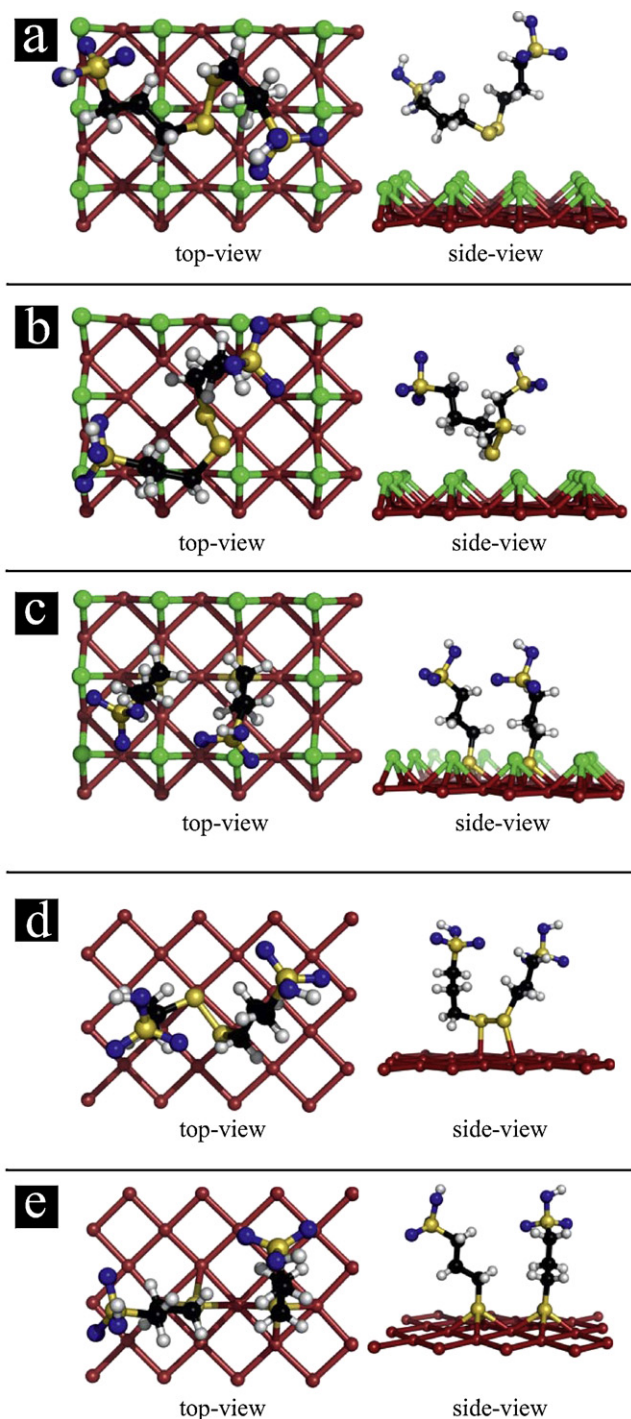


Fig. 7. (a)–(c) DFT calculation of the SPS adsorption in the presence of the Cu(100)– $c(2 \times 2)$ -Cl lattice, (a) SPS physisorption on the $c(2 \times 2)$ -Cl lattice; (b) SPS physisorption on Cu(100) at defects in the $c(2 \times 2)$ -Cl lattice; (c) dissociative SPS chemisorption at defects in the $c(2 \times 2)$ -Cl lattice; (d) and (e) DFT calculation of the SPS adsorption on the Cu(100)– (1×1) lattice, (d) SPS physisorption; (e) dissociative SPS chemisorption.

is diverse and multifunctional. It is actually the chemisorbed chloride that introduces an extra barrier for the MPS production [15] (see discussion of Fig. 7). In context of the Damascene process the chemisorbed chloride serves in addition as specific linker between the PAG polymers and the copper surface (not shown in Fig. 8). The formed PAG/Cl/Cu(I) suppressor ensemble thereby limits not only the access of cupric ions to the surface but further impedes inter-diffusion of SPS. Note that state-of-the-art PAG polymers reveal

significantly improved barrier properties with respect to SPS inter-diffusion [40] which has been pointed as being crucial for the temporal stability of the suppressor ensembles on the wafer surface and the upper side-walls of Damascene features upon plating.

The initial stage of SPS/copper interaction is clearly dominated by SPS physisorption on the chloride-modified surface (Fig. 2, step 1 in Fig. 8) as reported by Bae et al. [15] and Moffat et al. [16,17]. Physisorption preferentially occurs via the S–S disulfide functionality of the SPS while the sulfonic head groups are pointing away from the chloride-terminated copper surface (Fig. 7b). Those sulfonic head groups are important in the course of the MPS production since they introduce selectivity into the SPS/surface interaction. Note that any displacement of the sulfonic or sulfonate head groups of the SPS precursor by positively charged functionalities (e.g. $-\text{NR}_4^+$) would lead to an intra-molecular competition in the SPS interaction with the copper surface. The anion-cation pairing between the cationic head group and the chemisorbed chloride would overrule the interaction of the $-\text{S}-\text{S}-$ disulfide functional group with the copper surface thereby slowing down the rate of SPS dissociation. The latter is considered as the key step for its anti-suppressing action in context of the Damascene process. In fact, disulfide additives derivatized by cationic head groups do not show any anti-suppressing effect with respect to the PAG/Cu(I)/Cl suppressor ensemble.

SPS physisorbed on bare copper is metastable. It dissociates almost spontaneously leaving two chemisorbed MPS units behind (Fig. 7c, step 2 in Fig. 8). The S–Cu interaction is energetically clearly favored over the S–Cl bonding leading to an MPS accumulation on the copper surface at the expense of the chloride coverage which drops down in the course of the SPS dissociation reaction. The final MPS surface coverage amounts to $\Theta_{\text{MPS}} = 0.25 \text{ ML}$ in the presence of co-adsorbed chloride. In the resulting $c(2 \times 2)$ -Cl–MPS co-adsorption layer every second Cl anion of the pristine $c(2 \times 2)$ -Cl phase has been displaced (Fig. 3, step 3 in Fig. 8). The remaining chloride sub-lattice, however, serves as structural template for the co-adsorbed MPS units. Selective chloride desorption therefore leads to the structural break-down of the $c(2 \times 2)$ -Cl–MPS co-adsorption phase leaving a disordered MPS phase behind (Fig. 6).

Crucial for the described dissociation process are point defects in the pristine chloride matrix. We assume that the sources of those required defects are anion desorption/re-adsorption dynamics that are accelerated during the copper deposition/dissolution reaction. This hypothesis is in agreement with our experimental observation of an MPS/Cl phase formation that gets accelerated if we initiate cycles of copper dissolution and deposition reactions.

We identify the formed MPS as the actual anti-suppressor species in context of the Cu Damascene process. Important effects of the chemisorbed MPS are the partial removal of chloride from the surface and in addition the steric blocking of remaining chloride. It is the outer layer of sulfonic head groups in the Cl/MPS co-adsorption phase that is supposed to limit the access of PAG polymers to the chloride that is still present on the copper.

According to the CEAC model anti-suppressor species are needed that reveal a certain lateral mobility on the copper surface [2,4,39]. At first sight the strong chemisorption of the MPS would exclude its fast lateral diffusion on copper.

However, the same anion desorption/re-adsorption dynamics that allow the SPS precursor to adsorb on the copper (step 2, Fig. 8) could lead to a partial MPS desorption into the near surface electrolyte. In this scenario the copper deposition in the presence of SPS would therefore lead to an accumulation of free MPS in the near-surface electrolyte. Free MPS has certainly a higher lateral mobility compared to the chemisorbed MPS (step 4, Fig. 4). Note that the free MPS is only a transient species in the SPS reaction cycle. It shows a strong tendency to (re-)adsorb on the chloride modified copper surface as already discussed by Moffat et al. [16,17] and confirmed

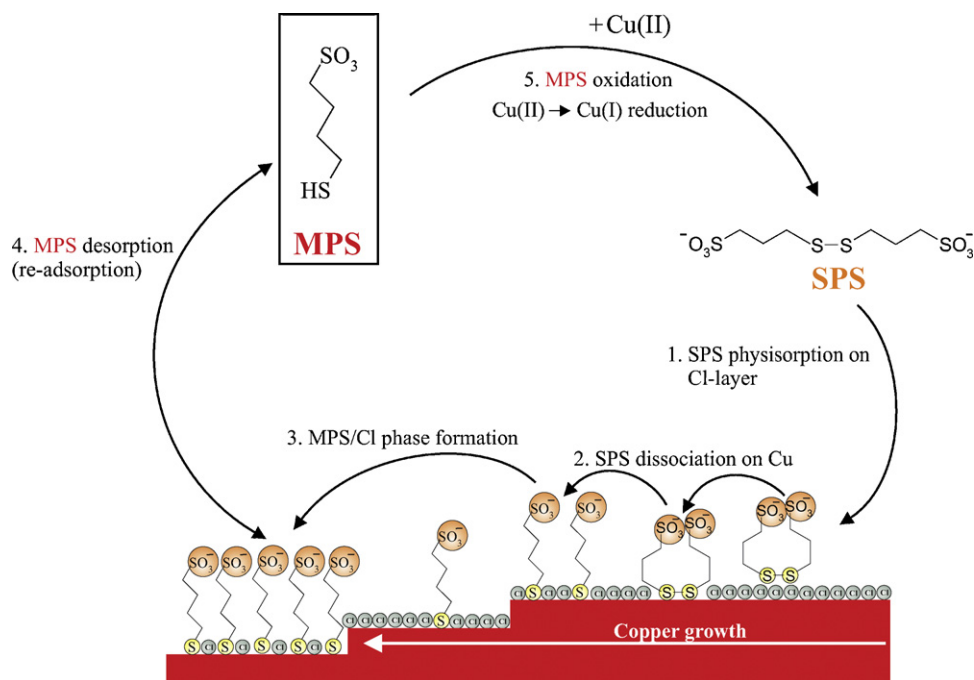


Fig. 8. Schematic representation of the SPS reaction cycle.

by our STM experiments (Figs. 3f–h). A further degradation pathway of the free MPS that closes the SPS reaction cycle (step 5 in Fig. 8) is the oxidative MPS dimerization to SPS provided Cu(II) is present in solution [43]. Thiolate-stabilized Cu(I) forms as by-product of this reaction. Hai et al. could recently indeed prove the SPS reaction cycle (SPS) involving the production of intermediate MPS and MPS-stabilized Cu(I) complexes as central to the understanding an oscillatory plating behavior when the SPS is combined with particular leveler additives [44].

5. Conclusions

We have studied the dissociative chemisorption of SPS on a chloride pre-covered Cu(1 0 0) model substrate by means of in situ STM and DFT. Our results demonstrate the importance of defect sites in the pristine the $c(2 \times 2)$ -Cl matrix for the dissociative SPS chemisorption. Defects can be generated under reactive conditions by accelerated anion desorption/re-adsorption dynamics in the course of copper dissolution and copper deposition. The formed Cl/MPS co-adsorption layer can be best described by a defect-rich $c(2 \times 2)$ -Cl-MPS phase where every second chloride anion of the pristine $c(2 \times 2)$ -Cl lattice is displaced by MPS units. Such a partial removal of chloride combined with a steric blocking of remaining chloride is discussed as central for the understanding of the anti-suppressing action of SPS in the course of the industrial Cu Damascene process.

Acknowledgment

P. Broekmann acknowledges the financial support by the Swiss National Foundation (SNF).

References

[1] P.C. Andricacos, C. Uzoh, J.O. Dukovic, J. Horkans, H. Deligianni, *IBM J. Res. Dev.* 42 (1998) 567.
 [2] T.P. Moffat, D. Wheeler, W.H. Huber, D. Josell, *Electrochim. Solid-State Lett.* 4 (2001) C26.

[3] T.P. Moffat, D. Wheeler, M.D. Edelstein, D. Josell, *IBM J. Res. Dev.* 49 (2005) 19.
 [4] T. Moffat, D. Wheeler, D. Josell, *ECS Trans.* 13 (2008) 129.
 [5] A.C. West, *J. Electrochem. Soc.* 147 (2000) 227.
 [6] R. Akolkar, U. Landau, *J. Electrochem. Soc.* 151 (2004) C702.
 [7] R. Akolkar, U. Landau, *J. Electrochem. Soc.* 156 (2009) D351.
 [8] J.W. Gallaway, A.C. West, *J. Electrochem. Soc.* 155 (2008) D632.
 [9] J. Mendez, R. Akolkar, U. Landau, *J. Electrochem. Soc.* 156 (2009) D474.
 [10] T.P. Moffat, D. Wheeler, D. Josell, *J. Electrochem. Soc.* 151 (2004) C262.
 [11] J.J. Kelly, A.C. West, *J. Electrochem. Soc.* 145 (1998) 3477.
 [12] Z.V. Feng, X. Li, A.A. Gewirth, *J. Phys. Chem. B* 107 (2003) 9415.
 [13] W.-P. Dow, M.-Y. Yen, C.-W. Liu, C.-C. Huang, *Electrochim. Acta* 53 (2008) 3610.
 [14] C.E. Taubert, D.M. Kolb, U. Memmert, H. Meyer, *J. Electrochem. Soc.* 154 (2007) D293.
 [15] S.-E. Bae, A.A. Gewirth, *Langmuir* 22 (2006) 10315.
 [16] T.P. Moffat, L.Y.O. Yang, *J. Electrochem. Soc.* 157 (2010) D228.
 [17] R.G. Brennan, M.M. Phillips, L.-Y.O. Yang, T.P. Moffat, *J. Electrochem. Soc.* 158 (2011) D178.
 [18] Q. Huang, B.C. Baker-O'Neal, J.J. Kelly, P. Broekmann, A. Wirth, C. Emnet, M. Martin, M. Hahn, A. Wagner, D. Mayer, *Electrochim. Solid-State Lett.* 12 (2009) D27.
 [19] M. Wilms, M. Kruff, G. Bermes, K. Wandelt, *Rev. Sci. Instrum.* 70 (1999) 3641.
 [20] M. Wilms, P. Broekmann, M. Kruff, Z. Park, C. Stuhlmann, K. Wandelt, *Surf. Sci.* 402 (1998) 83.
 [21] G. Kresse, J. Hafner, *Phys. Rev. B* 47 (1993) 558.
 [22] G. Kresse, J. Hafner, *Phys. Rev. B* 49 (1994) 14251.
 [23] G. Kresse, J. Furtmüller, *Phys. Rev. B* 54 (1996) 11169.
 [24] J.P. Perdew, K. Burke, M. Ernzerhof, *Phys. Rev. Lett.* 77 (1996) 3865.
 [25] G. Kresse, D. Joubert, *Phys. Rev. B* 59 (1999) 1758.
 [26] W. Reckien, B. Kirchner, F. Janetzko, T. Bredow, *J. Phys. Chem. C* 113 (2009) 10541.
 [27] S. Grimme, *J. Comput. Chem.* 27 (2006) 1787.
 [28] M. Saracino, P. Broekmann, K. Gentz, M. Becker, H. Keller, F. Janetzko, T. Bredow, K. Wandelt, H. Dosch, *Phys. Rev. B* 79 (2009) 115448.
 [29] D.W. Suggs, A.J. Bard, *J. Phys. Chem.* 99 (1995) 8349.
 [30] M.R. Vogt, A. Lachenwitzer, O.M. Magnussen, R.J. Behm, *Surf. Sci.* 399 (1998) 49.
 [31] S. Huemann, N.T. Minh Hai, P. Broekmann, K. Wandelt, H. Zajonz, H. Dosch, F. Renner, *J. Phys. Chem. B* 110 (2006) 24955.
 [32] H. Keller, M. Saracino, H.M.T. Nguyen, P. Broekmann, *Phys. Rev. B* 82 (2010) 245425.
 [33] P. Broekmann, M. Anastasescu, A. Spaenig, W. Lisowski, K. Wandelt, *J. Electroanal. Chem.* 500 (2001) 241.
 [34] N.T.M. Hai, W. Reckien, A. Flügel, W.M. Hahn, A. Wagner, D. Mayer, T. Bredow, P. Broekmann, 217th ECS Meeting Abstracts, #1248 (2010).
 [35] A. Taranovsky, T. Tansel, O.M. Magnussen, *Phys. Rev. Lett.* 104 (2010) 106101.
 [36] Y. Gruender, D. Kaminski, F. Golks, K. Krug, J. Stettner, O.M. Magnussen, A. Franke, J. Stremme, E. Pehlke, *Phys. Rev. B* 81 (2010) 174114.

- [37] A. Spaenig, P. Broekmann, K. Wandelt, *Z. Phys. Chem.* 217 (2003) 459.
- [38] J.J. Kelly, A.C. West, *J. Electrochem. Soc.* 145 (1998) 3472.
- [39] D. Josell, T.P. Moffat, D. Wheeler, *J. Electrochem. Soc.* 154 (2007) D208.
- [40] P. Broekmann, A. Fluegel, C. Emnet, M. Arnold, C. Roeger-Goepfert, A. Wagner, N.T.M. Hai, D. Mayer, *Electrochim. Acta* 56 (2011) 4724.
- [41] T.P. Moffat, D. Wheeler, S.K. Kim, D. Josell, *Electrochim. Acta* 53 (2007) 145.
- [42] T.P. Moffat, D. Wheeler, S.K. Kim, D. Josell, *J. Electrochem. Soc.* 153 (2006) C127.
- [43] J.P. Healy, D. Pletcher, M. Goodenough, *J. Electroanal. Chem.* 338 (1992) 167.
- [44] N.T.M. Hai, J. Odermatt, V. Grimaudo, K. Kraemer, A. Fluegel, M. Arnold, D. Mayer, P. Broekmann, *J. Phys. Chem. C*, doi:10.1021/jp2096086, in press.